OXFORD

SOT | Society of Toxicology
academic.oup.com/toxsci

TOXICOLOGICAL SCIENCES, 172(2), 2019, 265–278

doi: 10.1093/toxsci/kfz199
Dryad Digital Repository DOI: http://10.5061/dryad.qn8p2n0
Advance Access Publication Date: September 14, 2019
Research Article

Identification of Candidate Risk Factor Genes for Human Idelalisib Toxicity Using a Collaborative Cross Approach

Merrie Mosedale ,*,†,1,2 Yanwei Cai ,‡,1 John Scott Eaddy,* Robert W. Corty,‡ Manisha Nautiyal,* Paul B. Watkins ,*,† and William Valdar ‡,§

*Institute for Drug Safety Sciences, University of North Carolina at Chapel Hill, Research Triangle Park, North Carolina 27709; †Division of Pharmacotherapy and Experimental Therapeutics, UNC Eshelman School of Pharmacy, Chapel Hill, North Carolina 27599; and ‡Department of Genetics and §Lineberger Comprehensive Cancer Center, University of North Carolina at Chapel Hill, Chapel Hill, North Carolina 27599

[1]These authors contributed equally to this study.

[2]To whom correspondence should be addressed at UNC Eshelman School of Pharmacy, CB# 7569, Chapel Hill, NC 27599-7569. E-mail: merrie@unc.edu.

ABSTRACT

Idelalisib is a phosphatidylinositol 3-kinase inhibitor highly selective for the delta isoform that has shown good efficacy in treating chronic lymphocytic leukemia and follicular lymphoma. In clinical trials, however, idelalisib was associated with rare, but potentially serious liver and lung toxicities. In this study, we used the Collaborative Cross (CC) mouse population to identify genetic factors associated with the drug response that may inform risk management strategies for idelalisib in humans. Eight male mice (4 matched pairs) from 50 CC lines were treated once daily for 14 days by oral gavage with either vehicle or idelalisib at a dose selected to achieve clinically relevant peak plasma concentrations (150 mg/kg/day). The drug was well tolerated across all CC lines, and there were no observations of overt liver injury. Differences across CC lines were seen in drug concentration in plasma samples collected at the approximate T_{max} on study Days 1, 7, and 14. There were also small but statistically significant treatment-induced alterations in plasma total bile acids and microRNA-122, and these may indicate early hepatocellular stress required for immune-mediated hepatotoxicity in humans. Idelalisib treatment further induced significant elevations in the total cell count of terminal bronchoalveolar lavage fluid, which may be analogous to pneumonitis observed in the clinic. Genetic mapping identified loci associated with interim plasma idelalisib concentration and the other 3 treatment-related endpoints. Thirteen priority candidate quantitative trait genes identified in CC mice may now guide interrogation of risk factors for adverse drug responses associated with idelalisib in humans.

Key words: Collaborative Cross; drug-induced liver injury; idelalisib; precision medicine; toxicogenetics.

Idelalisib is a phosphatidylinositol 3-kinase inhibitor highly selective for the delta-isoform that has shown good efficacy in treating chronic lymphocytic leukemia and follicular lymphoma (Barrientos *et al.*, 2013; Graf and Gopal, 2016; Sharman *et al.*, 2014). Rare, but potentially serious drug-induced liver injury (DILI) was associated with idelalisib use in clinical trials (Castillo *et al.*, 2017; Lampson *et al.*, 2016). Pneumonitis and colitis were also observed, albeit to a lesser extent and not necessarily in the same patients experiencing hepatotoxicity. Studies to date have failed to identify highly predictive genetic risk factors that can inform risk management. As is the case with many DILI-causing drugs, nonclinical testing of idelalisib in traditional animal models (rats and dogs) did not indicate a risk for serious liver injury at clinically relevant concentrations (https://www.accessdata.fda.gov/drugsatfda_docs/nda/2014/205858Orig1s000PharmR.pdf; last accessed August 27, 2019). Dose-

dependent elevations in serum alanine aminotransferase (ALT) were observed in dog toxicology studies, but these were not accompanied by changes in histology and appeared to resolve over time with continued dosing.

Previous studies have demonstrated the ability of mouse genetic reference populations (GRPs) to model drug-induced injury in humans better than classical toxicology species (Harrill *et al.*, 2012). GRPs have also been utilized for pharmacogenomic analysis to identify risk factors associated with drug-induced adverse events in target organs (Church *et al.*, 2014, 2015; Harrill *et al.*, 2009, 2012; Mosedale *et al.*, 2014, 2017). Importantly, findings in GRP mice have been shown to translate to DILI risk factors in humans (Court *et al.*, 2014; Harrill *et al.*, 2009).

The Collaborative Cross (CC) is a recently developed and highly sophisticated GRP of multiparental recombinant inbred lines. This population was strategically designed to overcome limitations of classical inbred GRPs. The available set of CC lines have high genetic diversity, balanced allele frequencies, and dense, evenly distributed recombination sites (Collaborative Cross Consortium, 2012). A recent manuscript describes the utility of this population for identifying risk factors and mechanisms associated with the idiosyncratic DILI drug, tolvaptan (Mosedale *et al.*, 2017).

As with idelalisib, tolvaptan showed no hepatotoxic potential in traditional nonclinical animal models. Therefore, it was hypothesized that evaluating idelalisib-induced liver responses within the CC may help to identify lines sensitive to liver injury. These data could then be used to identify potential risk factors associated with susceptibility and provide a mechanistic understanding of this drug toxicity. Identifying risk factors and understanding mechanisms could inform risk management strategies for idelalisib and may also guide selection of next in class new drug candidates.

Unlike tolvaptan, where DILI onset occurred between 3 and 18 months (Watkins *et al.*, 2015), in clinical studies of idelalisib, ALT elevations were observed as early as 2 weeks on therapy. Therefore, it was hypothesized that a 14-day treatment regimen would be sufficient to elicit relevant toxicity phenotypes in mice. It should be noted that a once daily treatment regimen was also used in this study despite BID dosing in the clinic. This approach was selected to align with previous standard nonclinical studies from which toxicokinetic data were available (https://www.accessdata.fda.gov/drugsatfda_docs/nda/2014/205858Orig1s000PharmR.pdf and Gilead, unpublished internal data), and for logistical purposes.

MATERIALS AND METHODS

Animals

The CC is a panel of recombinant inbred lines derived from 8 inbred founder mouse strains (short names in parentheses): 129S1/SvlmJ (129S1), A/J (AJ), C57BL/6J (B6), NOD/ShiLtJ (NOD), NZO/HILtJ (NZO), CAST/EiJ (CAST), PWK/PhJ (PWK), and WSB/EiJ (WSB). The initiation of the CC breeding funnels, description of the CC lines, and animal housing are described elsewhere (Collaborative Cross Consortium, 2012). Eight male mice from each of 50 CC lines (listed on the x-axis of Figure 1) were purchased from the University of North Carolina, Chapel Hill (UNC). Care of the mice followed institutional guidelines under a protocol approved by the UNC Institutional Animal Care and Use Committee and standards set forth by the Guide for the Care and Use of Laboratory Animals. Animals were acclimated for approximately 7 days prior to dosing. At the initiation of treatment, mice were approximately 8–10 weeks of age.

In-life Procedures

Within each CC line, 4 animals were treated with vehicle (0.5% w/v carboxymethylcellulose and 0.1% v/v Tween 80 in purified water) and 4 were treated with idelalisib (150 mg/kg). Animals were assigned to treatment groups using a randomization method based on bodyweight. Vehicle- and idelalisib-treated animals within each line were treated in pairs, and pairs within each line were randomized over the course of the study to minimize batch (treatment group) effects. Test and control articles were administered daily by oral gavage in a dosing volume of 10 ml/kg for 14 days. Clinical assessments were performed at least once a day using previously described methods (Burkholder *et al.*, 2012). Animals were food fasted 17 h prior to dosing on study Days 1, 7, and 14 and continued fasting until after the 1 h post-dosing blood draw to control for food effects on exposure and bile acid levels. Approximately 100 μl of whole blood from each mouse was collected via puncture of the submandibular (facial) vein at 1 h post-dosing on study Days 1, 7, and 14. The blood was transferred to a tube containing K_2EDTA and centrifuged at 1300 × g and 4°C for 10 min to pellet red blood cells. Approximately 15 μl of plasma (idelalisib-treated animals only) was removed for analysis of drug concentration. Remaining supernatant (from all animals) was transferred to a clean microcentrifuge tube and centrifuged at 16 000 × g and 4°C for 10 min to pellet mitochondria for clinical chemistry analyses. Animals were food fasted 18 h prior to necropsy on study Day 15 to control for food effects on bile acid levels and reduce hepatic glycogen levels for improved histopathological assessment.

Necropsy

Animals were sacrificed 24 h after the last dose (on the morning of study Day 15) by CO_2 inhalation followed by cardiac exsanguination. Blood was collected by cardiac puncture, transferred into a microcentrifuge tube containing K_2EDTA, and processed as described above. The liver of each animal was removed and gross observations and liver weights recorded. A section of the left and median liver lobes was fixed in 10% neutral buffered formalin and processed for histological analysis. The lung was cannulated and rinsed 3× with 800 μl of 0.9% sodium chloride solution containing 2.6 mM EDTA to generate bronchoalveolar lavage fluid (BALF).

Plasma Drug Concentration

Plasma drug concentration was analyzed as previously described in Yao *et al.* (2018). Briefly, plasma samples were diluted twice and treated with acetonitrile. Mixtures were centrifuged at 4275 RPM for 15 min and supernatants were transferred to a 96-well plate for analysis using the API 5000 triple quadrupole mass spectrometer (AB Sciex).

Clinical Chemistry

Interim and terminal plasma levels of total bile acid (TBA) were determined using the Diazyme Total Bile Acids Assay (Poway, California) with a modified protocol corresponding to the Crystal Chem Total Bile Acids Kit (Downers Grove, Illinois). The assay was performed using a SpectraMax microtiter plate reader (Molecular Devices, Sunnyvale, California). Terminal plasma levels of microRNA-122 (miR-122) were assayed by qPCR using methods previously described in Mosedale *et al.* (2017). Terminal plasma levels of total and direct bilirubin (TBIL/DBIL) were measured on a SpectraMax microtiter plate reader using

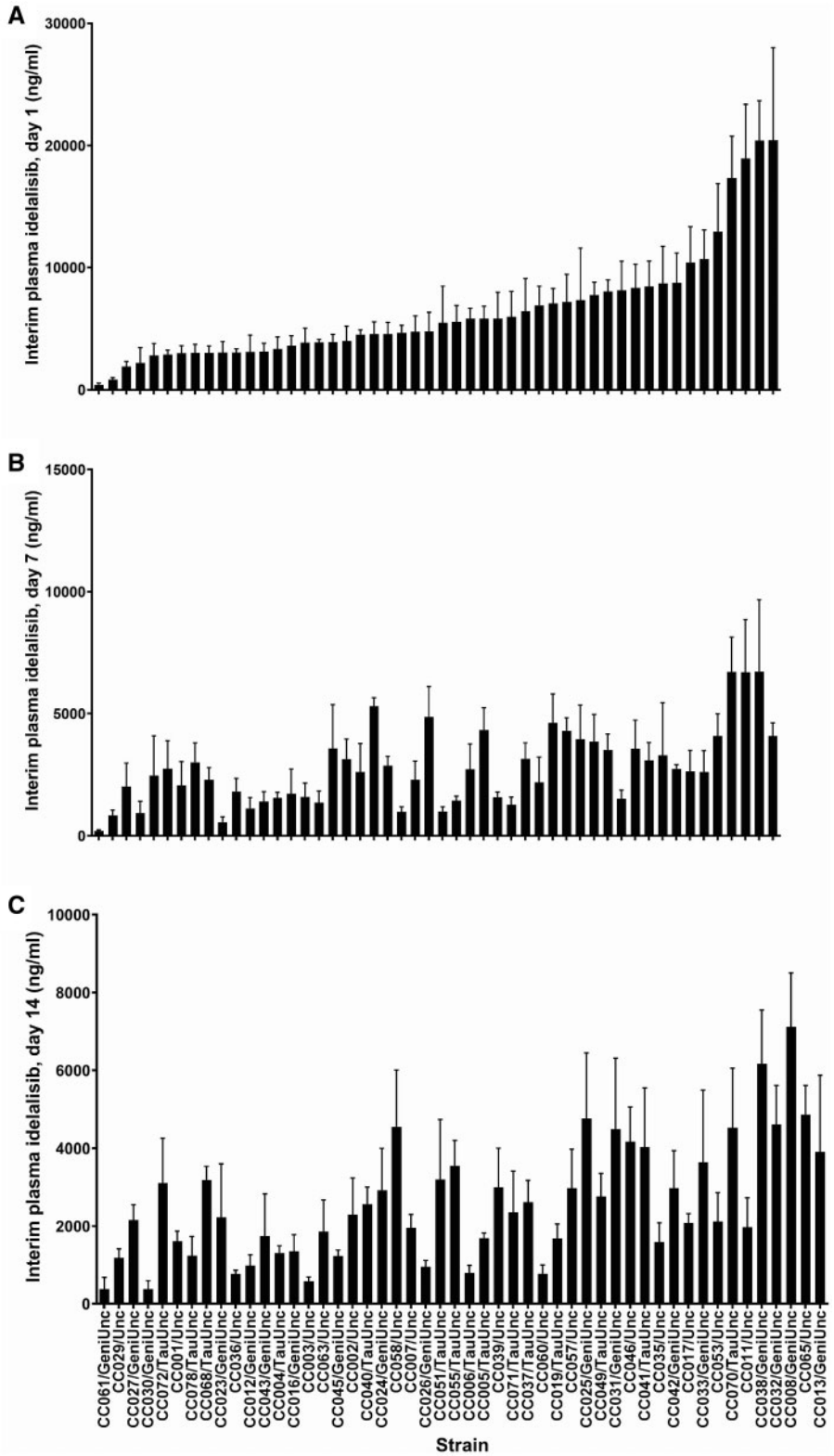

Figure 1. Average plasma idelalisib concentrations measured at 1 h post dose on study Days (A) 1, (B) 7, and (C) 14. Data are represented as mean + SEM of $N = 4$ idelalisib-treated animals except 1 animal with no sample on Day 1 (CC040/TauUnc) and 1 Collaborative Cross (CC) line with only 3 pairs of animals in the study (CC049/TauUnc). $P < .0001$ for the difference among log-transformed CC line means on each study day.

the Carolina Chemistries Total Bilirubin Reagent. Terminal plasma levels of glutamate dehydrogenase (GLDH), ALT, and aspartate aminotransferase (AST) were assessed using standard assays on a CLC 720 clinical chemistry analyzer (Carolina Liquid Chemistries, Winston-Salem, North Carolina).

Bronchoalveolar Lavage Fluid

Bronchoalveolar lavage fluid was centrifuged at 300 × g and 4°C for 5 min to pellet cells. The cell pellet was resuspended in Hank's Balanced Salt Solution. Cell counts were performed on the Cellometer (Nexcelom, Lawrence, Massachusetts) using AO/PI Staining Solution.

Histology

Formalin-fixed liver tissue was paraffin-embedded, cut into 5-μm sections and stained with hematoxylin and eosin (H&E). Hematoxylin and eosin stained slides were microscopically examined and scored by a Board-Certified Veterinary Pathologist (Charles River Laboratories, Pathology Associates).

Statistical Analysis of Phenotype Data

Statistical analyses on quantitative values were performed using GraphPad Prism statistical software version 8.0.1 (GraphPad Software, La Jolla, California). Fold change values were calculated by dividing each idelalisib-treated animal value by its corresponding vehicle-treated control. To analyze the effect of treatment across the whole population, log-transformed fold change values were averaged by CC line and values from all lines compared with a hypothetical mean of 0 using a 1-sample *t*-test. To analyze the effect of strain, log-transformed fold change values from all pairs were compared across strains using an ordinary 1-way ANOVA. A Pearson's correlation was used when comparing the log-transformed fold change values for clinical chemistry analytes to one another or to drug concentration. Group comparisons for clinical observations and gross and microscopic pathology data were made using nonstatistical methods.

Two vehicle-treated animals (CC065/Unc and CC071/TauUnc) died prematurely during the study and were excluded from the analysis of terminal endpoints. Both animals were sacrificed early in the study due to moribundity. The corresponding idelalisib-treated animals were also excluded from paired analysis. Only 3 pairs were used in CC049/TauUnc due to limited availability within the study timeline. Insufficient sample volume or values below the limit of quantitation resulted in the inability to obtain terminal endpoint values from other animals as noted.

Statistical Genetic Analysis

The statistical genetic analysis described below uses a set of related regression-based models to infer effects of idelalisib-response phenotypes that are based on the experimental pairing of idelalisib- and vehicle-treated mice described earlier. Formally, the *i*th (matched) pair is defined as comprising 2 mice of the same CC strain but of opposite treatment assignment, where treatment with vehicle or idelalisib occurred on the same dosing date. Letting y_i be the postdrug phenotype of idelalisib-treated mouse and $y_{i'}$ be the baseline phenotype of its vehicle-treated pair, the idelalisib response for pair *i* was defined as

$$\Delta_i = t(y_i) - t(y_{i'}), \tag{1}$$

where *t* is a normalizing transformation $\log_e$, such that Δ_i measures the log fold change between the 2 paired mice. In the case of drug concentration, where vehicle-treated animals were not analyzed $t(y_{i'})$ was defined as 0, such that $\Delta_i = t(y_i)$. Prior to quantitative trait loci (QTL) mapping, a linear model was used to regress out of the effects of batch on both types of measurements and the effect of drug concentration on idelalisib-response phenotypes; a correction for body-weight was unnecessary in this case because weights between each pair were similar by design.

Genotype and haplotype reconstruction of the CC mice. The genome of each CC line comprises a mosaic of haplotypes inherited from the 8 CC founders. This haplotype mosaic, which is typically inferred probabilistically from genotyping data, is the primary basis for QTL mapping in the CC. Data on specific variants, from the genotyping of the CC lines or available genotype and/or sequence data on the 8 founders, is then used in fine-mapping, that is, identification of candidate variants in QTL regions. The genome data for CC lines used in this study were obtained from the UNC Systems Genetics website: http://csbio.unc.edu/CCstatus/index.py. This resource provides haplotype mosaics estimated from genotyping of the CC using the 78K-marker "MegaMUGA" genotype platform (Morgan and Welsh, 2015). Briefly, probe intensities from MegaMUGA were converted using a hidden Markov model (HMM) (Fu *et al.*, 2012) into a probabilistic representation of the haplotype mosaic: the HMM calculates at each genotyped locus the probability of having inherited each of the 36 possible haplotype pairings (diplotypes). Diplotype probability data for the 51K reported shared markers were reduced to averaged data on 5111 genome "segments," achieved by averaging the probability matrices of each block of 10 consecutive markers. Analysis of this segmented data gave genome scans comparable with using all 51K markers, but at a 10th of the runtime, and with a reduced impact of genotyping errors (due to averaging). Genomic locations in genome scan were reported using NCBI mouse genome build 37.

Quantitative trait loci mapping. QTL mapping was performed by testing the association between idelalisib response and the inherited founder haplotypes at each point in the genome. For each line *s*, the idelalisib response was defined as the mean idelalisib response of its matched pairs, ie, $\Delta\text{mean}_s = 1/n_s \sum_{i \in \{i:s[i]=s\}} \Delta_i$, where $s[i]$ returns the strain of pair *i*, and where n_s is the number of observations for each line. Genetic association was tested by fitting at each genomic locus $m = 1, \ldots, 5111$, the weighted linear model,

$$\Delta\text{mean}_s = \text{QTL}_{sm} + \varepsilon_s, \tag{2}$$

where ε_s is the weighted residual error modeled as $\varepsilon_s \sim N(0, \sigma^2/n_s)$, and QTL_{sm} is the contribution of a QTL at locus *m*, defined as the sum of the effects of the founder haplotypes, weighted by the count of each haplotype. Specifically, for line *s*, this quantity is defined as

$$\text{QTL}_{sm} = \beta_{\text{AJ},m} x_{\text{AJ},sm} + \cdots + \beta_{\text{WSB},m} x_{\text{WSB},sm}, \tag{3}$$

where, for example, $\beta_{\text{AJ},m}$ is the effect of the AJ haplotype on idelalisib response, and $x_{\text{AJ},sm}$ is the number of founder AJ haplotypes present at locus *m* in CC line *s*. Because the haplotype counts $x_{\text{AJ},sm}, \ldots, x_{\text{WSB},sm}$ are not observed directly, being approximated only via the diplotype probabilities and therefore subject to uncertainty, QTL_{sm} was modeled using the multiple

imputation (MI) method described in Mosedale *et al.* (2017); in this method, the model above is refit to multiple (20) independent realizations (imputations) of the haplotype counts drawn from the distribution of the diplotype probabilities. At each imputation, the likelihood of the fitted model was compared with likelihood of the same model fitted with the QTL term swapped for a constant intercept (ie, the null model), with the resulting comparison yielding a likelihood ratio test p-value. The median of these p-values was used to represent association at the locus, with this quantity reported as the negative $\log_{10}$ value, $-\log_{10}(p)$. Genome-wide significance thresholds were calculated using a permutation procedure designed to control family-wide error rate. At each permutation, the genome scanning procedure described above was repeated but with the genome information of lines 1, 2,…, 49, 50 having been reassigned to a random reordering of those lines, eg, 28, 41,…, 13, 7; from this genome scan, the maximum $-\log_{10}(p)$ was then recorded. The maximum $-\log_{10}(p)$ for all permutations was used to fit a generalized extreme value distribution (Dudbridge and Koeleman, 2004), and the upper 5th percentile of this fitted distribution was taken as the 0.05 genome-wide significance threshold.

Haplotype effects at detected loci and confidence intervals for location. For detected QTL the effect of alternate haplotype substitutions on drug response was estimated using the Diploffect model of Zhang *et al.* (2014). This is a Bayesian hierarchical model that provides confidence intervals for both additive (haplotype) effects and dominance (heterozygous diplotype) effects, incorporating any uncertainty in the haplotype assignments from the HMM. Confidence intervals for the location of detected QTL were defined using positional bootstrapping after Visscher *et al.* (1996), as previously described in Phillippi *et al.* (2014) and Solberg Woods *et al.* (2012). To provide estimates that are computationally stable, 1000 nonparametric bootstraps were performed for each phenotype to obtain a distribution of highest peak positions and the 80% confidence interval was reported as the narrowest interval covering 80% of that distribution.

Multiallelic merge analysis in the 80% QTL confidence interval. To identify candidate variants within the 80% CI of a significant QTL peak we used a multiallelic version of "merge analysis" (Yalcin *et al.*, 2005). Merge analysis tests whether the QTL signal identified by haplotype association can be explained by the pattern of alleles at a known variant, comparing the fit of the 8-allele haplotype model with that of a simpler "merged" model in which haplotypes carrying the same variant allele are forced to have the same haplotype effect. For example, consider a variant with $k = 3$ alleles and strain distribution pattern 00111222, meaning that allele 0 is shared by the first 2 founders (129S1, AJ), allele 1 shared by the next 3 (B6, NOD, NZO) and allele 2 is in the last 3 founders (CAST, PWK, WSB). In the merged model for this variant, the QTL term in equation 3 would have only 3 effects, $\mathrm{QTL}_{sm} = \beta_0 x_0 + \beta_1 x_1 + \beta_2 x_2$, where, for example, $x_1 = x_{B6,sm} + x_{\mathrm{NOD},sm} + x_{\mathrm{NZO},sm}$.

Whereas the original version of merge analysis considered only biallelic merges, corresponding to testing imputed single nucleotide polymorphisms (SNPs), here we used a multiallelic version, generalizing the number of alleles from 2 to $k = 2,\ldots,7$, and thereby accommodating multiallelic variants such as copy number variants. Information on known imputed variants in the CC lines was drawn from the Inbred Strain Variant database (https://isvdb.unc.edu) (Oreper *et al.*, 2017), which imputes this information by combining diplotype probabilities for the CC strain genomes with variant data on the CC founders from the Wellcome Trust Sanger Institute's Mouse Genomes Project (http://www.sanger.ac.uk/resources/mouse/genomes/). Prior to the merge analysis, filtering was performed to remove SNPs with poor variant calling and non-informative strain distribution patterns across the 8 CC founder strains (eg, where all 8 founder strains have the same allele). At each variant within the 80% CI, p values from the merged model were compared with those from the 8-allele haplotype model; an equal or stronger association from the merged model was considered to be consistent with the target variant explaining the haplotype association and thus being a candidate driver of the QTL.

Expression quantitative trait loci analysis. For QTL where all candidate SNPs were intergenic, candidate quantitative trait genes (QTGs) were identified using the baseline CC expression QTL (eQTL) data described in Mosedale *et al.* (2017). Idelalisib response phenotypes, merge analysis results, and phenotype expression correlations have been deposited in the Dryad Digital Repository under the DOI: 10.5061/dryad.qn8p2n0.

RESULTS

Plasma Idelalisib Concentrations Vary Among Collaborative Cross Mice

Plasma idelalisib concentrations were measured on study Days 1, 7, and 14 at 1h post-dose, the approximate time of peak plasma concentrations (T_{max}) in mice (Gilead, unpublished internal data). Although idelalisib dose was adjusted for bodyweight, the average plasma concentration of idelalisib varied significantly by CC line on each study day (Figure 1). All interim plasma idelalisib measurements were highly correlated ($p < .0001$ and $r = 0.537$–0.564 for log-transformed values, Pearson correlation), but there was an overall drop in the median of average concentrations across the CC lines from Day 1 (5138 ng/ml) to Days 7 (2634 ng/ml) and 14 (2257 ng/ml). Median concentrations on Days 7 and 14 were comparable with peak plasma concentrations (C_{max}) observed in previous mouse and human studies (based on unpublished internal data, Gilead and clinical pharmacology studies reviewed in https://www.accessdata.fda.gov/drugsatfda_docs/nda/2014/205858Orig1s000ClinPharmR.pdf; last accessed August 27, 2019), and the sum of these values was used for subsequent analyses. Plasma idelalisib concentrations were near 0 in most CC lines at 24 h post-dose measured on study Day 15 (Supplementary Figure 1).

Idelalisib Induces Small but Statistically Significant Changes in Biomarkers of Liver and Lung Injury in Collaborative Cross Mice

The 14-day treatment regimen of idelalisib was well tolerated across all CC lines. Clinical findings were observed sporadically or at approximately the same incidence in vehicle- and idelalisib-treated animals, and there were no clear idelalisib-related macroscopic or microscopic findings in the livers of CC mice. However, idelalisib treatment was associated with small but statistically significant effects on 5 of 10 plasma biomarkers of liver injury measured in this study: interim and terminal TBA, miR-122, GLDH, and ALT (Table 1). Idelalisib treatment was also associated with a significant effect on terminal BALF cell count, a biomarker for lung injury that was measured in this study. A trend toward differences in the fold change of the treatment-induced effects across CC lines was observed for many of these biomarkers, although none reached statistical significance (Table 1). Average fold change compared with

Table 1. Treatment and Strain Effects for Toxicity Biomarkers

Phenotype	Treatment (p Value)	Strain (p Value)	Median (Fold Change)	Minimum (Fold Change)	Maximum (Fold Change)
Interim TBA, Day 1	**0.0639**	**0.0719**	1.680	0.1923	14.83
Interim TBA, Day 7	**0.0015**	0.6680	1.025	0.4075	17.16
Interim TBA, Day 14	0.0845	**0.0332**	1.281	0.1875	15.97
Terminal TBA	**0.0298**	0.6284	1.276	0.2675	44.47
Terminal miR-122	**0.0110**	0.2187	1.159	0.2200	8.418
Terminal TBIL	0.3723	0.4318	1.129	0.7000	2.475
Terminal DBIL	0.1034	0.0699	1.180	0.6025	4.430
Terminal GLDH	**0.0177**	0.7662	1.020	0.5100	2.873
Terminal ALT	**0.0056**	0.6096	0.9850	0.6775	1.455
Terminal AST	0.6314	0.2692	1.055	0.7375	2.560
Terminal BALF	**0.0015**	0.9795	1.436	0.6616	7.757

p-values and descriptive statistics for log-transformed fold change compared with paired control values for plasma total bile acid (TBA), microRNA 122 (miR-122), total bilirubin (TBIL), direct bilirubin (DBIL), glutamate dehydrogenase (GLDH), alanine aminotransferase (ALT), aspartate aminotransferase (AST), and bronchoalveolar lavage fluid (BALF) cell count. Phenotypes with statistically significant effects and the associated p values are highlighted in bold.

paired control plotted by strain for all liver and lung biomarkers are shown in Supplementary Figure 2.

Genetic Mapping of Plasma Idelalisib Concentrations Identifies a Significant Association on Chromosome 17

Genetic mapping was used to identify genomic regions whose variation might underlie variability in the idelalisib phenotypes measured across the CC lines evaluated here. Initially, QTL mapping was performed using plasma idelalisib concentrations to determine if genetic factors influence exposure, which could in turn impact the liver and lung response. Genome scans were performed using log-transformed values for all individual interim and terminal plasma idelalisib measurements as well as combinations of these data. No significant QTL were identified using the terminal data. However, the same significantly associated locus on chromosome 17 was observed for the analyses of all 3 interim measurements, and therefore further interrogation of this peak utilized the scan resulting from the sum of plasma idelalisib concentrations measured at interim time points on study Days 7 and 14 (Figure 2A), as described previously.

Founder strain probabilities at the QTL peak (43.87 Mb, nominal $-\log_{10}(p) = 6.102654$) show an overrepresentation of NOD DNA among the mice with the lowest plasma idelalisib concentrations (Figure 2B). Bayesian modeling of the QTL haplotype effects estimated a strong negative effect of the NOD haplotype on plasma idelalisib concentrations (Figure 2C). The plasma idelalisib concentration QTL was mapped to an 80% confidence interval $<$ 3 Mb (43.673–46.201) (Figure 2D). This region was interrogated further to identify QTGs that may explain the differences in drug concentration.

Initially, candidate causal variants were identified using merge analysis (Phillippi *et al.*, 2014; Vered *et al.*, 2014; Yalcin *et al.*, 2005). Merge analysis compares the significance of association for individual variants obtained from the haplotype model used for genome-wide analysis with those obtained using a genotype model, where the founder strain haplotypes are "merged" into fewer than 8 groups according to their genotype, for example, 2 groups for each biallelic SNP. For potentially causative variants, both models will explain a significant portion of the variation, but the biallelic model will do so with far fewer parameters, providing a more parsimonious fit and more significant p-value. In the plasma idelalisib QTL region on chromosome 17 (43.673–46.201 Mb), 1691 variants were identified having a $-\log_{10}(p)$ from merge analysis greater than $-\log_{10}(p)$ from MIs and a $-\log_{10}(p)$ from merge analysis greater than 4 (Figure 2E). Of the variants meeting these criteria, the most abundantly represented strain distribution patterned was NOD discordant from all other founder strains (Figure 2F). In total, 64 unique genes were represented among the 1691 variants identified by merge analysis. Four priority candidate QTGs have human orthologs, are expressed in the liver, and have variants associated with differences in pharmacokinetics and/or pharmacodynamics and are thus considered priority candidate QTGs for further investigation: ATP-binding cassette, subfamily C, member 10 (*Abcc10*), cytochrome P450, family 39, subfamily a, polypeptide 1 (*Cyp39a1*), nuclear factor of kappa light polypeptide gene enhancer in B cells inhibitor, epsilon (*Nfkbie*), and solute carrier family 22, member 7 (*Slc22a7*). Although gene expression analysis was not performed in this study, expression data from vehicle-treated mice of the CC lines overlapping with Mosedale *et al.* (2017) were interrogated to determine the relationship between baseline candidate QTG mRNA levels and plasma idelalisib concentrations measured here. Of the 4 QTGs, only *Abcc10* transcript levels were found to be significantly correlated with the plasma idelalisib concentrations (r = -0.38, p = .023 for log-transformed values, Pearson correlation).

Genetic Mapping of Idelalisib Liver Responses Identifies Significant Associations for Two Plasma Biomarkers of Early Injury

Next, genetic mapping was performed using the idelalisib responses for each of the endpoints reported in Table 1. Phenotypic values were corrected for drug concentration to enable the identification of genetic factors influencing idelalisib response independent of differences in exposure. Significant QTL were identified for 2 plasma biomarkers of early liver injury. A significant QTL on chromosome 8 was associated with log(fold change) interim plasma TBA concentrations measured on Day 1 (Figure 3A). Founder strain probabilities at the QTL peak (50.422 Mb, nominal $-\log_{10}(p) = 5.534508$) (Figure 3B) and Bayesian modeling of the QTL haplotype effects (Figure 3C) suggest that multiple haplotypes contribute to idelalisib-induced alterations in plasma TBA. The plasma TBA QTL was mapped to an 80% confidence interval $<$ 2 Mb (49.408–50.997 Mb) (Figure 3D). Merge analysis was performed but did not identify candidate QTGs for interim plasma TBA fold change (Supplementary Figure 3). Instead, expression data from vehicle-treated CC mice in Mosedale *et al.* (2017) was used to identify 22 transcripts with eQTLs in the confidence interval for

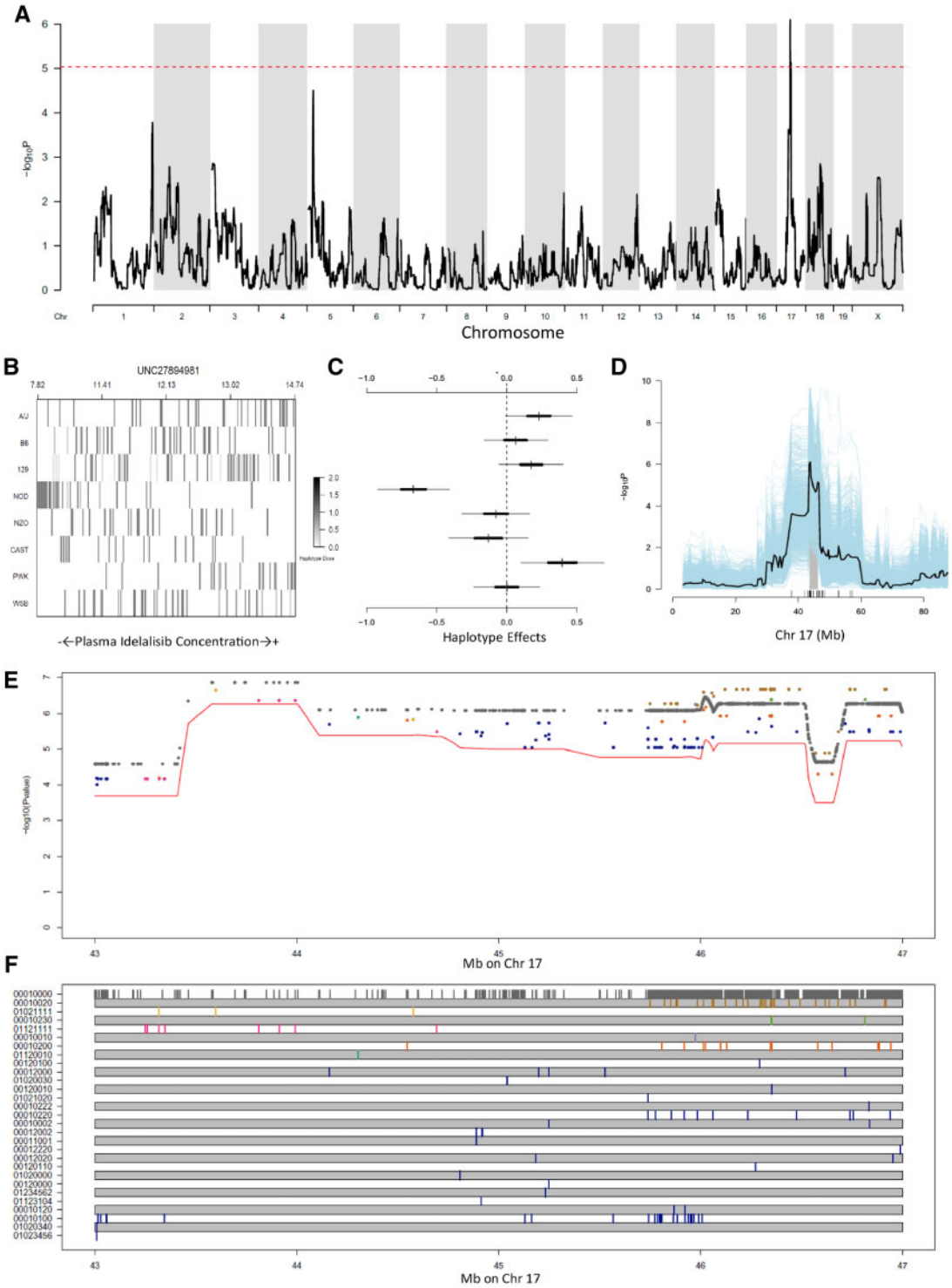

Figure 2. (A) Genome scan plot illustrating quantitative trait loci (QTL) associated with the sum of interim plasma idelalisib concentrations measured on Days 7 and 14. Dashed horizontal line indicates genome-wide significance at the 0.05 level. (B) Founder strain probabilities at the locus peak. The x-axis plots paired animals in order from left to right by increasing log(plasma idelalisib concentrations). Each horizontal row indicates the probability of a given Collaborative Cross founder haplotype being present at the locus, with darker intensities indicating higher probabilities (0–1.0). (C) Estimates and confidence intervals for haplotype substitution effects at the peak locus. (D), Confidence interval plot for the QTL on chromosome 17. The 80% confidence interval (Chr17: 43.673–46.201 Mb) is indicated by gray shading. (E) Comparison of $-\log_{10}(p)$ values from 8-allele haplotype model (line) to $-\log_{10}(p)$ values from 2-allele merge analysis (dots) for variants in the 80% confidence interval with a $-\log_{10}(p)$ from merge analysis merge analysis $>$ $-\log_{10}(p)$ from 8-allele haplotype model and a $-\log_{10}(p)$ from merge analysis > 4. (F) Corresponding strain distribution pattern for variants represented in E. Each track corresponds to strain distribution pattern indicated in the left margin by a string of integers representing the alleles for the 8 founder strains, in the order: A/J, B6, 129, NOD, NZO, CAST, PWK, and WSB. Within each SDP track, the vertical lines indicate the locations of the variants within the strain distribution pattern.

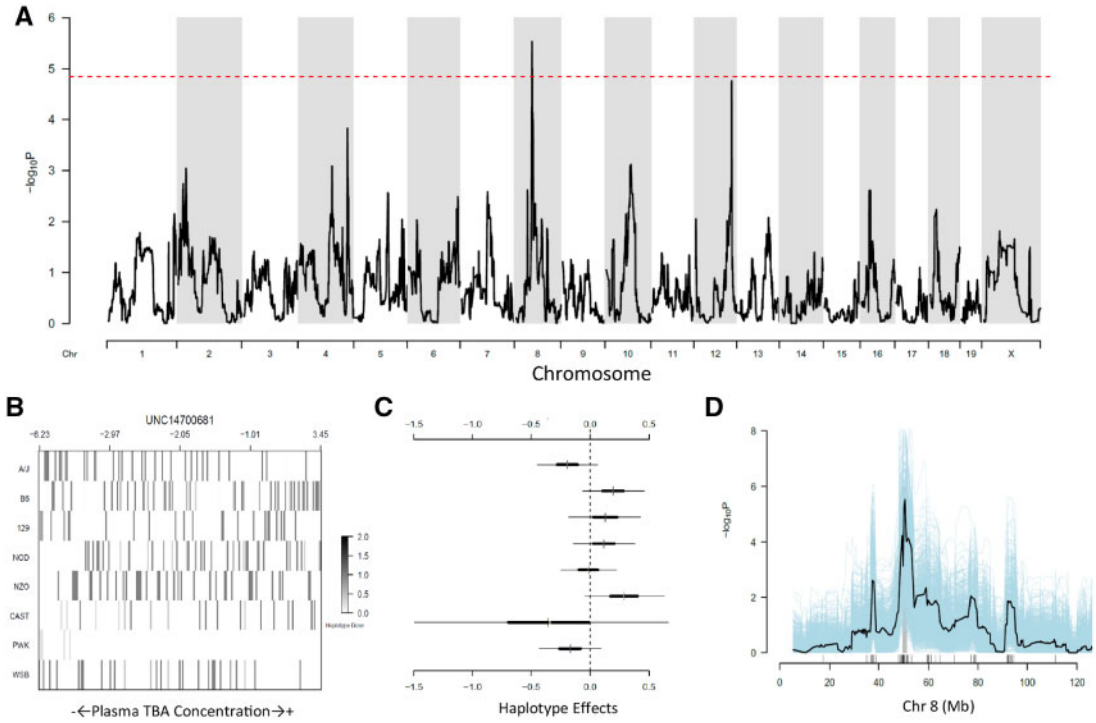

Figure 3. (A) Genome scan plot illustrating quantitative trait loci (QTL) associated with log(fold change) in interim plasma total bile acid (TBA) concentrations measured on Day 1. Dashed horizontal line indicates genome-wide significance at the 0.05 level. (B) Founder strain probabilities at the locus peak. The x-axis plots paired animals in order from left to right by increasing log(fold change plasma TBA). Each horizontal row indicates the probability of a given Collaborative Cross founder haplotype being present at the locus, with darker intensities indicating higher probabilities (0–1.0). (C) Estimates and confidence intervals for haplotype substitution effects at the peak locus. (D) Confidence interval plot for the QTL on chromosome 8. The 80% confidence interval is indicated by gray shading.

the TBA QTL on chromosome 8. Three priority candidate QTGs have human orthologs, are expressed in the liver, and have variants associated with differences in cholesterol and/or bile acid biosynthesis are thus considered priority candidate QTGs for further investigation: cytochrome P450 family 51 subfamily A member 1 (*Cyp51*), 3-hydroxy-3-methylglutaryl-CoA reductase (*Hmgcr*), and sterol carrier protein 2 (*Scp2*). Baseline mRNA levels for these candidate QTGs measured in Mosedale *et al.* (2017) were not significantly correlated with plasma TBA concentrations measured here.

A significant QTL was also identified for terminal log(fold change) plasma miR-122 on chromosome X (Figure 4A). Founder strain probabilities at the QTL peak (136.492 Mb, nominal $-\log_{10}(p) = 5.020391$) (Figure 4B) and Bayesian modeling of the QTL haplotype effects (Figure 4C) suggest that multiple haplotypes contribute to idelalisib-induced alterations in plasma miR-122. The plasma TBA QTL was mapped to an 80% confidence interval approximately 10 Mb (127–136.492 Mb) (Figure 4D). Merge analysis was performed but did not identify candidate QTGs for interim plasma TBA fold change (Supplementary Figure 4). Instead, expression data from vehicle-treated CC mice in Mosedale *et al.* (2017) was used to identify 37 transcripts with eQTLs in the confidence interval for the TBA QTL on chromosome 8. Four priority candidate QTGs have human orthologs, are expressed in the liver, and have variants associated with liver injury and/or mechanisms of liver injury and are thus considered priority candidate QTGs for further investigation: 5′-aminolevulinate synthase 2 (*Alas2*), ATP synthase, H+ transporting, mitochondrial F1 complex, alpha subunit 1 (*Atp5a1*), and HECT, UBA, and WWE domain containing 1 (*Huwe1*), E3 ubiquitin protein ligase (*Ubash3a*). Baseline mRNA levels for these candidate genes measured in Mosedale *et al.* (2017) were not significantly correlated with miR-122 concentrations measured here.

Genetic Mapping Also Identifies a Significant Association for a Possible Lung Injury Phenotype

Finally, genetic mapping was performed using log(fold change) values for BALF cell count and a significant QTL was identified on chromosome 3 (Figure 5A). Founder strain probabilities at the QTL peak (117.258 Mb, nominal $-\log_{10}(p) = 4.688878$) show an overrepresentation of A/J and CAST DNA among the mice with the highest BALF cell count fold change values (Figure 5B). Bayesian modeling of the QTL haplotype effects estimated a strong positive effect of the A/J and CAST haplotypes on plasma idelalisib concentrations (Figure 5C). The BALF cell count QTL was mapped to an 80% confidence interval approximately 45 Mb (99.617–145.711 Mb) (Figure 5D). This region was interrogated further to identify QTGs that may explain the differences in the lung phenotype.

In the BALF cell count QTL region on chromosome 3 (99.617–145.711 Mb), 844 variants were identified having a $-\log_{10}(p)$ from merge analysis greater than $-\log_{10}(p)$ from MIs and a $-\log_{10}(p)$ from merge analysis greater than 4 (Figure 5E). Of the variants meeting these criteria, the most abundantly represented strain distribution patterned was A/J and CAST discordant from all other founder strains (Figure 5F). In total, 25 unique genes were represented among the 844 variants identified by merge analysis. Two priority candidate QTGs have human orthologs, are expressed in the lung, and have

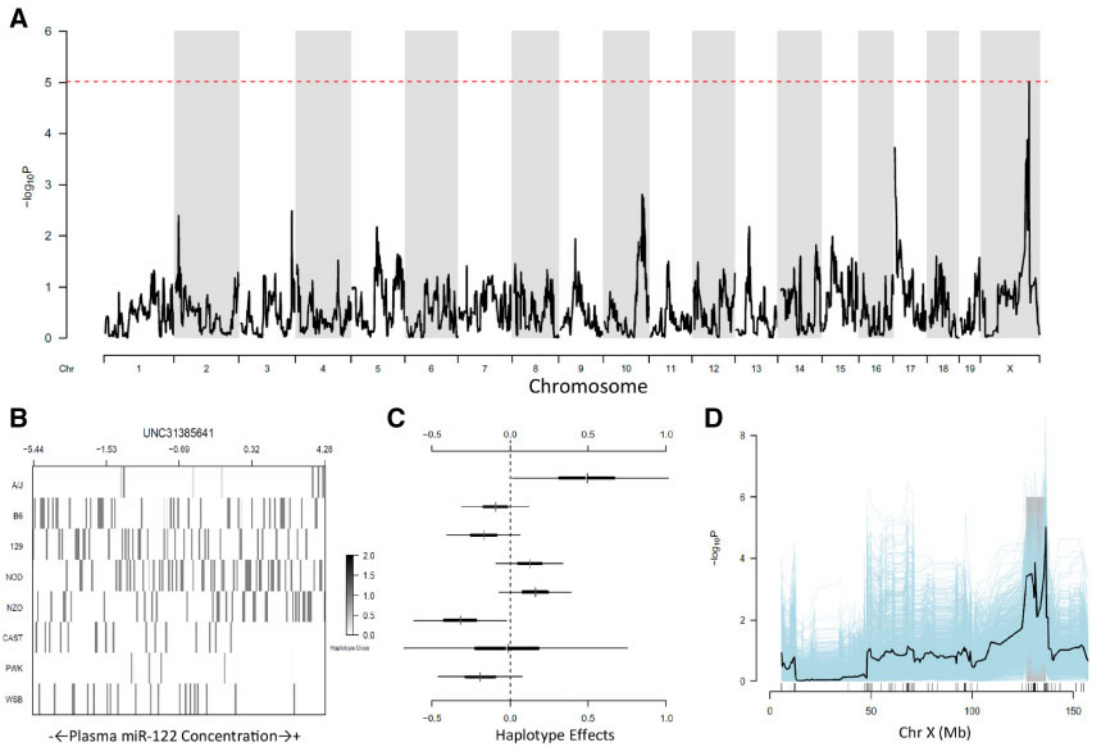

Figure 4. (A) Genome scan plot illustrating quantitative trait loci (QTL) associated with log(fold change) in terminal plasma miR-122 concentrations. Dashed horizontal line indicates genome-wide significance at the 0.05 level. (B) Founder strain probabilities at the locus peak. The x-axis plots paired animals in order from left to right by increasing log(fold change plasma miR-122). Each horizontal row indicates the probability of a given Collaborative Cross founder haplotype being present at the locus, with darker intensities indicating higher probabilities (0–1.0). (C) Estimates and confidence intervals for haplotype substitution effects at the peak locus. (D) Confidence interval plot for the QTL on chromosome X. The 80% confidence interval is indicated by gray shading.

variants associated with lung inflammation are thus considered priority candidate QTGs for further investigation: glutathione S-transferase, mu 1 (*Gstm1*) and vascular cell adhesion molecule 1 (*Vcam1*). Baseline mRNA levels for these candidate genes measured in Mosedale *et al.* (2017) were not significantly correlated with BALF cell counts measured here.

DISCUSSION

The decrease in plasma idelalisib concentrations from Day 1 to Day 7 observed in this study has not been reported in other nonclinical or clinical studies. This suggests that the genetic diversity represented among CC mice may allow for the observation of unique aspects of idelalisib metabolism. Similarly, the range of plasma idelalisib concentrations observed across CC lines is a novel observation and suggests that genetic factors may contribute to differences in idelalisib pharmacokinetics. This is supported by genetic mapping which identified a significant QTL associated with interim plasma idelalisib concentrations.

Four high priority candidate QTGs were identified for the QTL associated with plasma idelalisib concentrations, including human orthologs of 3 DMET genes and a transcriptional regulator of DMET genes. ABCC10 is a member of the multidrug resistance protein subfamily reported to transport several anticancer drugs (Zhang *et al.*, 2017). *Abcc1*−/− mice are hypersensitive to paclitaxel toxicity due to increased cellular drug accumulation (Hopper-Borge *et al.*, 2011). In humans, the ABCC10 SNP rs9349256 is associated with increased tenofovir-induced kidney toxicity (Pushpakom *et al.*, 2011), and rs2125739 is associated with lower nevirapine plasma concentrations (Liptrott *et al.*, 2012). CYP39A1 is an ER protein primarily involved in the conversion of cholesterol to bile acids (Li-Hawkins *et al.*, 2000). The CYP39A1 SNP rs7761731 is associated with increased docetaxel-induced leukopenia and infection (Melchardt *et al.*, 2015), and rs9381468 and rs953062 are associated with decreased busulfan clearance (ten Brink *et al.*, 2013). NFKBIE regulates NFkB (Hoffmann *et al.*, 2002; Li and Nabel, 1997), which in turn regulates the expression of a number of ADME genes, and in humans variants (both SNPs and deletions) are associated with several disease states. Also the NFKBIE SNP rs2233434 is associated with decreased cellular methotrexate uptake via regulation of SLC19A1 (Imamura *et al.*, 2016). Finally, SLC22A7 is a sodium-independent organic anion transporter (OAT2) (Sekine *et al.*, 1998). The SLC22A7 SNP rs4149178 is associated with increased capecitabine-induced (Pellicer *et al.*, 2017) and anthracycline (daunorubicin and doxorubicin)-induced cardiotoxicity (Visscher *et al.*, 2015). The SLC22A7 SNP rs2270860 is associated with increased capecitabine-induced skin toxicity (Pellicer *et al.*, 2017). Among CC lines, variants in these genes are associated with lower plasma idelalisib concentration.

The relationship between plasma idelalisib C_{max} and susceptibility to liver injury in the clinic is not known. However, it appears that most adverse drug reactions are dose-dependent, even if the relationship is not obvious within the therapeutic range (Uetrecht and Naisbitt, 2013). Therefore, genetic factors influencing variability in idelalisib pharmacokinetics may be relevant to adverse reactions observed in the clinic. Furthermore, the pathogenesis of idelalisib liver injury may be multifactorial involving events at both the level of the hepatocyte and the immune system, and thus differences in pharmacokinetics may be relevant to early hepatocellular events that are necessary but not sufficient to support overt liver injury.

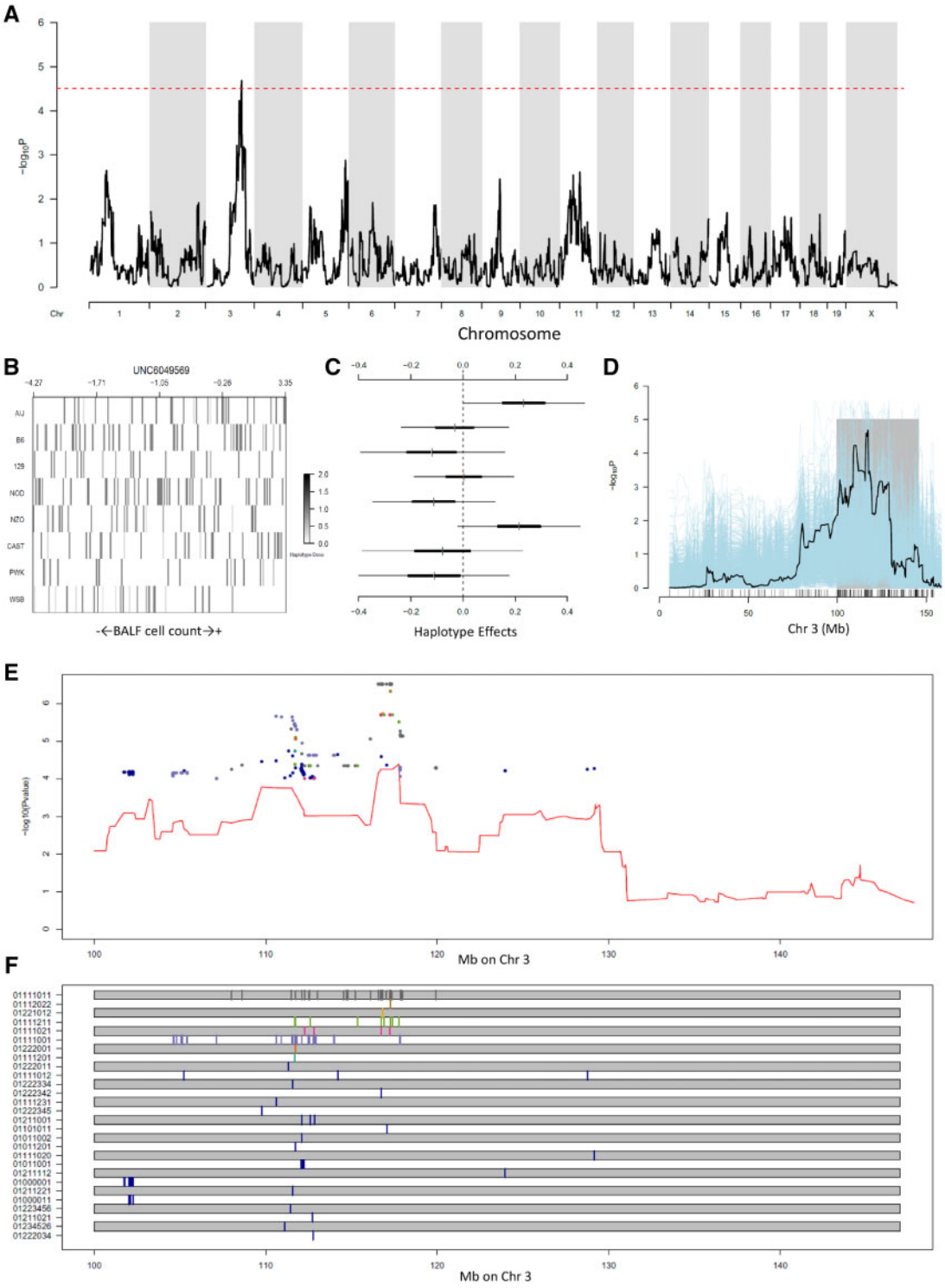

Figure 5. (A) Genome scan plot illustrating quantitative trait loci (QTL) associated with the log(fold change) of terminal bronchoalveolar lavage fluid (BALF) cell count. Dashed horizontal line indicates genome-wide significance at the 0.05 level. (B) Founder strain probabilities at the locus peak. The x-axis plots paired animals in order from left to right by increasing log(fold change BALF cell count). Each horizontal row indicates the probability of a given Collaborative Cross founder haplotype being present at the locus, with darker intensities indicating higher probabilities (0–1.0). (C) Estimates and confidence intervals for haplotype substitution effects at the peak locus. (D) Confidence interval plot for the QTL on chromosome 3. The 80% confidence interval (Chr3: 99.617–145.711 Mb) is indicated by gray shading. (E) Comparison of $-\log_{10}(p)$ values from 8-allele haplotype model (line) to $-\log_{10}(p)$ values from 2-allele merge analysis (dots) for variants in the 80% confidence interval with a $-\log_{10}(p)$ from merge analysis merge analysis $>$ $-\log_{10}(p)$ from 8-allele haplotype model and a $-\log_{10}(p)$ from merge analysis > 4. (F) Corresponding strain distribution pattern for variants represented in E. Each track corresponds to strain distribution pattern indicated in the left margin by a string of integers representing the alleles for the 8 founder strains, in the order: A/J, B6, 129, NOD, NZO, CAST, PWK, and WSB. Within each SDP track, the vertical lines indicate the locations of the variants within the strain distribution pattern.

Interestingly, SNPs in human orthologs of candidate QTGs for plasma idelalisib concentration described here occur at a minor allele frequency similar to the prevalence of liver injury associated with idelalisib in the clinic.

The lack of robust liver-related findings observed in CC mice could be due to the shorter treatment regimen used in this study compared with the clinical protocol. It may also reflect lower exposures achieved in this study compared with clinical trials. Median interim plasma idelalisib concentrations in the CC mice were comparable with clinic values where grade $\geq$ 3 ALT elevations have been observed in approximately 14% of patients (Coutre *et al.*, 2015). However, due to rapid metabolism, exposures in mice are reportedly much lower than those observed in humans (unpublished observations reported in Carter *et al.*, 2017; Palazzo *et al.*, 2018). Furthermore, clinical protocols typically use BID dosing, which results in an overall higher AUC in humans. Finally, the absence of liver injury in CC mice may be due to species-specific differences in the mechanism of toxicity and/or in susceptibility factors required to elicit overt hepatotoxicity.

A recent study suggests that the liver injury associated with idelalisib in clinical trials is in part due to an on-target, immune-mediated event (Lampson *et al.*, 2016). Phosphatidylinositol 3-kinase delta (PI3KD) is critical for the function of $CD4^+CD25^+Foxp3^+$ regulator T-cells (Tregs) (Patton *et al.*, 2006), and Tregs have been shown to play an important role in modulating DILI in mouse models (Chen *et al.*, 2015; Mak and Uetrecht, 2015; Metushi *et al.*, 2015). Unfortunately, due to unfavorable pharmacokinetic properties (Carter *et al.*, 2017; Palazzo *et al.*, 2018), data on the pharmacological activity of idelalisib in mice are limited. Nonetheless, significant evidence suggests that although overt hepatotoxicity is the result of a T-cell response, the cascade of events culminating in immune-mediated DILI begins with off-target, drug-induced hepatocyte stress, the release of danger signals, and activation of the innate immune system (Mosedale and Watkins, 2017). In the case of idelalisib, this is supported by the lack of any reported liver injury in PI3KD mutant mice (Okkenhaug *et al.*, 2002; Uno *et al.*, 2010). Importantly, these early hepatocellular events can occur in the absence of overt toxicity and may be detected by measuring biomarkers of early cell stress (Mosedale et al., 2018).

In this study, significant QTL were identified for idelalisib-induced changes in 2 plasma biomarkers associated with hepatocyte stress in CC mice: interim TBA and terminal miR-122. Elevations in plasma bile acids can reflect inhibition of bile acid transport into bile, which can result in a toxic accumulation of bile acids in the hepatocyte and impaired mitochondrial ATP production (Schadt *et al.*, 2016). miR-122 is a more sensitive and specific marker of liver injury, and also a danger signal that when released in hepatocyte-derived exosomes can signal to and activate the innate immune system (Momen-Heravi *et al.*, 2015).

Three high priority candidate genes involved in cholesterol and bile acid biosynthesis had eQTLs in the phenotype QTL for plasma TBA: CYP51A1, HMGCR, and SCP2. At 5 weeks of age, liver-specific *Hmgcr*−/− mice show severe hepatic steatosis with apoptotic cells, hypercholesterolemia, and hypoglycemia (Nagashima *et al.*, 2012). *Scp2*−/− mice have altered bile flow and lower bile salt secretion rates (Nagashima *et al.*, 2012). Four high priority candidate genes associated with liver injury or mechanisms of liver injury had eQTLs in the phenotype QTL for plasma miR-122: ALAS2, ATP5A1, HUWE1, and UBASH3A. In response to immune challenge, *Ubash3a*−/− mice have increased inflammation and T-cell response (Newman *et al.*, 2014; San Luis *et al.*, 2011). SNPs in all these genes are associated with relevant phenotypes in humans, but more importantly, validated eQTLs have also been described. In the CC lines, variants in the TBA and miR-122 phenotype QTLs for idelalisib are associated with differential expression of these genes.

Finally, small but statistically significant elevations in BALF total cell count were observed in response to idelalisib treatment. This phenotype may inform risk factors associated with pneumonitis also observed in a smaller percentage of idelalisib-treated patients in clinical trials (Coutre *et al.*, 2015). Two high priority candidate genes were identified for the QTL associated with plasma idelalisib concentrations. GSTM1 functions in the detoxification of electrophilic compounds, including carcinogens, therapeutic drugs, environmental toxins, and products of oxidative stress, by conjugation with glutathione. *Gstm1*−/− mice have low GST activity which alters toxicological responses to a variety of drugs. In humans, GSTM1 is highly polymorphic (only expressed in 50% of individuals) and variations can impact susceptibility to carcinogens as well as the toxicity and efficacy of certain drugs (Board *et al.*, 1990). GSTM1 null genotypes also associated with increased sensitivity to diesel exhaust particle-induced allergic airway inflammation (Gilliland *et al.*, 2004) and COPD development and severity (Malic *et al.*, 2017). VCAM1 is a cell surface glycoprotein expressed by cytokine-activated endothelium, mediates the adhesion of monocytes and lymphocytes. Cleavage is associated with pulmonary vascular endothelial activation and soluble form is elevated in BALF of patients with acute respiratory distress syndrome (Attia *et al.*, 2016). VCAM1 is TGF-β1 inducible and upregulated in lungs of subjects with idiopathic pulmonary fibrosis (Agassandian *et al.*, 2015). VCAM1 SNPs rs3783611, rs114207303, and rs3783615 are associated with increased VCAM1-dependent monocyte adhesion (Schmitz *et al.*, 2013). VCAM1 SNP rs3176860 is associated with increased neutrophil and CRP levels in blood (Yu *et al.*, 2017). And VCAM1 SNP rs3783605 is associated with several VCAM1-related diseases increases VCAM1 expression (Dadgar Pakdel *et al.*, 2015). In the CC lines, variants in these genes are associated with higher idelalisib-induced BALF cell counts.

In conclusion, the 14-day treatment regimen of idelalisib was well tolerated across all CC lines. Although idelalisib dose was adjusted for bodyweight, differences in plasma drug concentration were observed among genetically different CC lines. Idelalisib treatment-induced alterations in plasma TBA and miR-122 in mouse may indicate early hepatocellular stress required for immune-mediated hepatotoxicity in humans. Small but statistically significant elevations in terminal BALF total cell count were also observed in response to idelalisib treatment in CC mice, which may be analogous to pneumonitis observed in the clinic. Candidate genes identified for the QTLs associated with these phenotypes can now guide interrogation of risk factors for adverse drug responses associated with idelalisib in humans.

SUPPLEMENTARY DATA

Supplementary data are available at *Toxicological Sciences* online.

DECLARATION OF CONFLICTING INTERESTS

The author/authors declared no potential conflicts of interest with respect to the research, authorship, and/or publication of this article.

ACKNOWLEDGMENTS

We would like to thank multiple core facilities at University of North Carolina Chapel Hill for their assistance. We extend our gratitude to: Darla Miller and the team of the UNC System Genetic Core for their assistance with the Collaborative Cross mice and the in-life study; Charlene Santos and the team of the UNC Animal Studies Core for their assistance with the in-life study; and Rachel Church of the UNC Organ Injury Biomarker Core for her assistance with BALF cell counts and assay development for other organ injury biomarkers. We would also like to thank Stacey Tannheimer and Joseph Therrien of Gilead for assistance with study design and analytical work.

FUNDING

This work was supported by funding received from Gilead Sciences, Inc. Animal Studies were performed within the UNC Lineberger Animal Studies Core Facility at the University of North Carolina at Chapel Hill. The UNC Lineberger Animal Studies Core is supported in part by an NCI Center Core Support (CA16086) to the UNC Lineberger Comprehensive Cancer Center. W.V. and (partially) Y.C. were supported by a National Institute of General Medical Sciences (R35-GM127000).

REFERENCES

Agassandian, M., Tedrow, J. R., Sembrat, J., Kass, D. J., Zhang, Y., Goncharova, E. A., Kaminski, N., Mallampalli, R. K., and Vuga, L. J. (2015). VCAM-1 is a TGF-beta1 inducible gene upregulated in idiopathic pulmonary fibrosis. *Cell. Signal.* **27**, 2467–2473.

Attia, E. F., Jolley, S. E., Crothers, K., Schnapp, L. M., and Liles, W. C. (2016). Soluble vascular cell adhesion molecule-1 (sVCAM-1) is elevated in bronchoalveolar lavage fluid of patients with acute respiratory distress syndrome. *PLoS One* **11**, e0149687.

Barrientos, J. C., Furman, R. R., Leonard, J., Flinn, I., Rai, K. R., De Vos, S., Schreeder, M. T., Wagner-Johnston, N. D., Sharman, J. P., and Boyd, T. E. (2013). Update on a phase I study of the selective PI3Kδ inhibitor idelalisib (GS-1101) in combination with rituximab and/or bendamustine in patients with relapsed or refractory CLL. *J. Clin. Oncol.* **31**, 7017–7017.

Board, P., Coggan, M., Johnston, P., Ross, V., Suzuki, T., and Webb, G. (1990). Genetic heterogeneity of the human glutathione transferases: A complex of gene families. *Pharmacol. Ther.* **48**, 357–369.

Burkholder, T., Foltz, C., Karlsson, E., Linton, C. G., and Smith, J. M. (2012). Health evaluation of experimental laboratory mice. *Curr. Protoc. Mouse Biol.* **2**, 145–165.

Carter, M. J., Cox, K. L., Blakemore, S. J., Turaj, A. H., Oldham, R. J., Dahal, L. N., Tannheimer, S., Forconi, F., Packham, G., and Cragg, M. S. (2017). PI3Kdelta inhibition elicits anti-leukemic effects through Bim-dependent apoptosis. *Leukemia* **31**, 1423–1433.

Castillo, J. J., Gustine, J. N., Meid, K., Dubeau, T., Yang, G., Xu, L., Hunter, Z. R., and Treon, S. P. (2017). Idelalisib in Waldenstrom macroglobulinemia: High incidence of hepatotoxicity. *Leuk. Lymphoma* **58**, 1002–1004.

Chen, T., Gao, J., Xiang, P., Chen, Y., Ji, J., Xie, P., Wu, H., Xiao, W., Wei, Y., Wang, S., *et al.* (2015). Protective effect of platycodin D on liver injury in alloxan-induced diabetic mice via regulation of Treg/Th17 balance. *Int. Immunopharmacol.* **26**, 338–348.

Church, R. J., Gatti, D. M., Urban, T. J., Long, N., Yang, X., Shi, Q., Eaddy, J. S., Mosedale, M., Ballard, S., Churchill, G. A., *et al.* (2015). Sensitivity to hepatotoxicity due to epigallocatechin gallate is affected by genetic background in diversity outbred mice. *Food Chem. Toxicol.* **76**, 19–26.

Church, R. J., Wu, H., Mosedale, M., Sumner, S. J., Pathmasiri, W., Kurtz, C. L., Pletcher, M. T., Eaddy, J. S., Pandher, K., Singer, M., *et al.* (2014). A systems biology approach utilizing a mouse diversity panel identifies genetic differences influencing isoniazid-induced microvesicular steatosis. *Toxicol. Sci.* **140**, 481–492.

Collaborative Cross Consortium. (2012). The genome architecture of the Collaborative Cross mouse genetic reference population. *Genetics* **190**, 389–401.

Court, M. H., Peter, I., Hazarika, S., Vasiadi, M., Greenblatt, D. J., and Lee, W. (2014). Candidate gene polymorphisms in patients with acetaminophen-induced acute liver failure. *Drug Metab. Dispos.* **42**, 28–32.

Coutre, S., Barrientos, J. C., Brown, J. R., De Vos, S., Furman, R. R., Keating, M. J., O'Brien, S. M., Pagel, J. M., Sharman, J. P., Zelenetz, A. D., *et al.* (2015). Safety of idelalisib in B-cell malignancies: Integrated analysis of eight clinical trials. *J. Clin. Oncol.* **33**, e18030.

Dadgar Pakdel, F., Keramatipour, M., Noorbakhsh, F., Talebi, S., and Vodjgani, M. (2015). Investigating the effect of rs3783605 single-nucleotide polymorphism on the activity of VCAM-1 promoter in human umbilical vein endothelial cells. *Iranian J. Allergy Asthma Immun.* **14**, 179–87.

Dudbridge, F., and Koeleman, B. P. C. (2004). Efficient computation of significance levels for multiple associations in large studies of correlated data, including genomewide association studies. *Am. J. Hum. Genet.* **75**, 424–435.

Fu, C.-P., Welsh, C. E., de Villena, F. P.-M., and McMillan, L. (2012). Inferring ancestry in admixed populations using microarray probe intensities. In *Proceedings of the ACM Conference on Bioinformatics, Computational Biology and Biomedicine–BCB '12*, pp. 105–112. ACM, New York, NY.

Gilliland, F. D., Li, Y. F., Saxon, A., and Diaz-Sanchez, D. (2004). Effect of glutathione-S-transferase M1 and P1 genotypes on xenobiotic enhancement of allergic responses: Randomised, placebo-controlled crossover study. *Lancet (London, England)* **363**, 119–125.

Graf, S. A., and Gopal, A. K. (2016). Idelalisib for the treatment of non-Hodgkin lymphoma. *Expert Opin. Pharmacother.* **17**, 265–274.

Harrill, A. H., DeSmet, K. D., Wolf, K. K., Bridges, A. S., Eaddy, J. S., Kurtz, C. L., Hall, J. E., Paine, M. F., Tidwell, R. R., and Watkins, P. B. (2012). A mouse diversity panel approach reveals the potential for clinical kidney injury due to DB289 not predicted by classical rodent models. *Toxicol. Sci.* **130**, 416–426.

Harrill, A. H., Watkins, P. B., Su, S., Ross, P. K., Harbourt, D. E., Stylianou, I. M., Boorman, G. A., Russo, M. W., Sackler, R. S., Harris, S. C., *et al.* (2009). Mouse population-guided resequencing reveals that variants in CD44 contribute to acetaminophen-induced liver injury in humans. *Genome Res.* **19**, 1507–1515.

Hoffmann, A., Levchenko, A., Scott, M. L., and Baltimore, D. (2002). The IκB-NF-κB signaling module: Temporal control and selective gene activation. *Science* **298**, 1241–1245.

Hopper-Borge, E. A., Churchill, T., Paulose, C., Nicolas, E., Jacobs, J. D., Ngo, O., Kuang, Y., Grinberg, A., Westphal, H., Chen, Z.-S., *et al.* (2011). Contribution of Abcc10 (Mrp7) to *in vivo*

paclitaxel resistance as assessed in Abcc10(−/−) mice. *Cancer Res*. **71**, 3649–3657.

Imamura, H., Yoshina, S., Ikari, K., Miyazawa, K., Momohara, S., and Mitani, S. (2016). Impaired NFKBIE gene function decreases cellular uptake of methotrexate by down-regulating SLC19A1 expression in a human rheumatoid arthritis cell line. *Mod. Rheumatol.* **26**, 507–516.

Lampson, B. L., Kasar, S. N., Matos, T. R., Morgan, E. A., Rassenti, L., Davids, M. S., Fisher, D. C., Freedman, A. S., Jacobson, C. A., Armand, P., *et al.* (2016). Idelalisib given front-line for treatment of chronic lymphocytic leukemia causes frequent immune-mediated hepatotoxicity. *Blood* **128**, 195–203.

Li, Z., and Nabel, G. J. (1997). A new member of the I kappaB protein family, I kappaB epsilon, inhibits RelA (p65)-mediated NF-kappaB transcription. *Mol. Cell. Biol.* **17**, 6184–6190.

Li-Hawkins, J., Lund, E. G., Bronson, A. D., and Russell, D. W. (2000). Expression cloning of an Oxysterol 7α-hydroxylase selective for 24-hydroxycholesterol. *J. Biol. Chem.* **275**, 16543–16549.

Liptrott, N. J., Pushpakom, S., Wyen, C., Fätkenheuer, G., Hoffmann, C., Mauss, S., Knechten, H., Brockmeyer, N. H., Hopper-Borge, E., Siccardi, M., *et al.* (2012). Association of ABCC10 polymorphisms with nevirapine plasma concentrations in the German Competence Network for HIV/AIDS. *Pharmacogenet. Genomics* **22**, 10–19.

Mak, A., and Uetrecht, J. (2015). The combination of anti-CTLA-4 and PD1−/− mice unmasks the potential of isoniazid and nevirapine to cause liver injury. *Chem. Res. Toxicol.* **28**, 2287–2291.

Malic, Z., Topic, A., Francuski, D., Stankovic, M., Nagorni-Obradovic, L., Markovic, B., and Radojkovic, D. (2017). Oxidative stress and genetic variants of xenobiotic-metabolising enzymes associated with COPD Development and Severity in Serbian adults. *J. Chron. Obstruct. Pulm. Dis.* **14**, 95–104.

Melchardt, T., Hufnagl, C., Magnes, T., Weiss, L., Hutarew, G., Neureiter, D., Schlattau, A., Moser, G., Gaggl, A., Tränkenschuh, W., *et al.* (2015). CYP39A1 polymorphism is associated with toxicity during intensive induction chemotherapy in patients with advanced head and neck cancer. *BMC Cancer* **15**, 725.

Metushi, I. G., Hayes, M. A., and Uetrecht, J. (2015). Treatment of PD-1−/− mice with amodiaquine and anti-CTLA4 leads to liver injury similar to idiosyncratic liver injury in patients. *Hepatology*. **61**, 1332–42.

Momen-Heravi, F., Bala, S., Kodys, K., and Szabo, G. (2015). Exosomes derived from alcohol-treated hepatocytes horizontally transfer liver specific miRNA-122 and sensitize monocytes to LPS. *Sci. Rep.* **5**, 9991.

Morgan, A. P., and Welsh, C. E. (2015). Informatics resources for the Collaborative Cross and related mouse populations. *Mamm. Genome* **26**, 521–539.

Mosedale, M., Eaddy, J. S., Trask, J. O. J., Holman, N. S., Wolf, K. K., LeCluyse, E., Ware, B. R., Khetani, S. R., Lu, J., Brock, W. J., *et al.* (2018). miR-122 release in exosomes precedes overt tolvaptan-induced necrosis in a primary human hepatocyte micropatterned coculture model. *Toxicol. Sci.* **161**, 149–158.

Mosedale, M., Kim, Y., Brock, W. J., Roth, S. E., Wiltshire, T., Eaddy, J. S., Keele, G. R., Corty, R. W., Xie, Y., Valdar, W., *et al.* (2017). Editor's highlight: Candidate risk factors and mechanisms for tolvaptan-induced liver injury are identified using a Collaborative Cross approach. *Toxicol. Sci.* **156**, 438–454.

Mosedale, M., and Watkins, P. B. (2017). Drug-induced liver injury: Advances in mechanistic understanding that will inform risk management. Invited "state-of-the-art" review. *Clin. Pharmacol. Ther.* **101**, 469–480.

Mosedale, M., Wu, H., Kurtz, C. L., Schmidt, S. P., Adkins, K., and Harrill, A. H. (2014). Dysregulation of protein degradation pathways may mediate the liver injury and phospholipidosis associated with a cationic amphiphilic antibiotic drug. *Toxicol. Appl. Pharmacol.* **280**, 21–29.

Nagashima, S., Yagyu, H., Ohashi, K., Tazoe, F., Takahashi, M., Ohshiro, T., Bayasgalan, T., Okada, K., Sekiya, M., Osuga, J., *et al.* (2012). Liver-specific deletion of 3-hydroxy-3-methylglutaryl coenzyme A reductase causes hepatic steatosis and death. *Arterioscler. Thromb. Vasc. Biol.* **32**, 1824–1831.

Newman, T. N., Liverani, E., Ivanova, E., Russo, G. L., Carpino, N., Ganea, D., Safadi, F., Kunapuli, S. P., and Tsygankov, A. Y. (2014). Members of the novel UBASH3/STS/TULA family of cellular regulators suppress T-cell-driven inflammatory responses *in vivo*. *Immunol. Cell Biol.* **92**, 837–850.

Okkenhaug, K., Bilancio, A., Farjot, G., Priddle, H., Sancho, S., Peskett, E., Pearce, W., Meek, S. E., Salpekar, A., Waterfield, M. D., *et al.* (2002). Impaired B and T cell antigen receptor signaling in p110delta PI 3-kinase mutant mice. *Science* **297**, 1031–1034.

Oreper, D., Cai, Y., Tarantino, L. M., de Villena, F. P.-M., and Valdar, W. (2017). Inbred strain variant database (ISVdb): A repository for probabilistically informed sequence differences among the Collaborative Cross strains and their founders. *Genes Genomes Genet.* **7**, 1623–1630.

Palazzo, A., Herter, S., Grosmaire, L., Jones, R., Frey, C. R., Limani, F., Bacac, M., Umana, P., Oldham, R. J., Marshall, M. J. E., *et al.* (2018). The PI3Kdelta-selective inhibitor idelalisib minimally interferes with immune effector function mediated by rituximab or obinutuzumab and significantly augments B cell depletion *in vivo*. *J. Immunol. (Baltimore, MD: 1950)* **200**, 2304–2312.

Patton, D. T., Garden, O. A., Pearce, W. P., Clough, L. E., Monk, C. R., Leung, E., Rowan, W. C., Sancho, S., Walker, L. S. K., Vanhaesebroeck, B., *et al.* (2006). Cutting edge: The phosphoinositide 3-kinase p110δ is critical for the function of CD4+CD25+Foxp3+ regulatory T cells. *J. Immunol.* **177**, 6598–6602.

Pellicer, M., Garcia-Gonzalez, X., Garcia, M. I., Robles, L., Gravalos, C., Garcia-Alfonso, P., Pachon, V., Longo, F., Martinez, V., Blanco, C., *et al.* (2017). Identification of new SNPs associated with severe toxicity to capecitabine. *Pharmacol. Res.* **120**, 133–137.

Phillippi, J., Xie, Y., Miller, D. R., Bell, T. A., Zhang, Z., Lenarcic, A. B., Aylor, D. L., Krovi, S. H., Threadgill, D. W., de Villena, F. P.-M., *et al.* (2014). Using the emerging Collaborative Cross to probe the immune system. *Genes Immun.* **15**, 38–46.

Pushpakom, S. P., Liptrott, N. J., Rodríguez-Nóvoa, S., Labarga, P., Soriano, V., Albalater, M., Hopper-Borge, E., Bonora, S., Di Perri, G., Back, D. J., *et al.* (2011). Genetic variants of ABCC10, a novel tenofovir transporter, are associated with kidney tubular dysfunction. *J. Infect. Dis.* **204**, 145–153.

San Luis, B., Sondgeroth, B., Nassar, N., and Carpino, N. (2011). Sts-2 is a phosphatase that negatively regulates zeta-associated protein (ZAP)-70 and T cell receptor signaling pathways. *J. Biol. Chem.* **286**, 15943–15954.

Schadt, H. S., Wolf, A., Pognan, F., Chibout, S.-D., Merz, M., and Kullak-Ublick, G. A. (2016). Bile acids in drug induced liver injury: Key players and surrogate markers. *Clin. Res. Hepatol. Gastroenterol.* **40**, 257–266.

Schmitz, B., Vischer, P., Brand, E., Schmidt-Petersen, K., Korb-Pap, A., Guske, K., Nedele, J., Schelleckes, M., Hillen, J.,

Rotrige, A., *et al.* (2013). Increased monocyte adhesion by endothelial expression of VCAM-1 missense variation *in vitro*. *Atherosclerosis* **230**, 185–190.

Sekine, T., Cha Seok, H., Tsuda, M., Apiwattanakul, N., Nakajima, N., Kanai, Y., and Endou, H. (1998). Identification of multispecific organic anion transporter 2 expressed predominantly in the liver. *FEBS Lett.* **429**, 179–182.

Sharman, J. P., Coutre, S. E., Furman, R. R., Cheson, B. D., Pagel, J. M., Hillmen, P., Barrientos, J. C., Zelenetz, A. D., Kipps, T. J., Flinn, I. W., *et al.* (2014). Second interim analysis of a phase 3 study of idelalisib (ZYDELIG®) plus rituximab (R) for relapsed chronic lymphocytic leukemia (CLL): Efficacy analysis in patient subpopulations with Del(17p) and other adverse prognostic factors. *Blood* **124**, 330.

ten Brink, M. H., van Bavel, T., Swen, J. J., van der Straaten, T, Bredius, R. G. M., Lankester, A. C., Zwaveling, J., and Guchelaar, H.-J. (2013). Effect of genetic variants GSTA1 and CYP39A1 and age on busulfan clearance in pediatric patients undergoing hematopoietic stem cell transplantation. *Pharmacogenomics* **14**, 1683–1690.

Uetrecht, J., and Naisbitt, D. J. (2013). Idiosyncratic adverse drug reactions: Current concepts. *Pharmacol. Rev.* **65**, 779–808.

Uno, J. K., Rao, K. N., Matsuoka, K., Sheikh, S. Z., Kobayashi, T., Li, F., Steinbach, E. C., Sepulveda, A. R., Vanhaesebroeck, B., Balfour Sartor, R., *et al.* (2010). Altered macrophage function contributes to colitis in mice defective in the phosphoinositide-3 kinase subunit p110δ. *Gastroenterology* **139**, 1642–1653.e1646.

Vered, K., Durrant, C., Mott, R., and Iraqi, F. A. (2014). Susceptibility to klebsiella pneumoniae infection in Collaborative Cross mice is a complex trait controlled by at least three loci acting at different time points. *BMC Genomics* **15**, 865.

Visscher, H., Rassekh, S. R., Sandor, G. S., Caron, H. N., van Dalen, E. C., Kremer, L. C., van der Pal, H. J., Rogers, P. C., Rieder, M. J., Carleton, B. C., *et al.* (2015). Genetic variants in SLC22A17 and SLC22A7 are associated with anthracycline-induced cardiotoxicity in children. *Pharmacogenomics* **16**, 1065–1076.

Visscher, P. M., Thompson, R., and Haley, C. S. (1996). Confidence intervals in QTL mapping by bootstrapping. *Genetics* **143**, 1013–1020.

Watkins, P., Lewis, J., Kaplowitz, N., Alpers, D., Blais, J., Smotzer, D., Krasa, H., Ouyang, J., Torres, V., Czerwiec, F., *et al.* (2015). Clinical pattern of tolvaptan-associated liver injury in subjects with autosomal dominant polycystic kidney disease: Analysis of clinical trials database. *Drug Saf.* **38**, 1103–1113.

Woods, L. C. S., Holl, K. L., Oreper, D., Xie, Y., Tsaih, S.-W., and Valdar, W. (2012). Fine-mapping diabetes-related traits, including insulin resistance, in heterogeneous stock rats. *Physiol. Genomics* **44**, 1013–1026.

Yalcin, B., Flint, J., and Mott, R. (2005). Using progenitor strain information to identify quantitative trait nucleotides in outbred mice. *Genetics* **171**, 673–681.

Yao, H., Price, T. T., Cantelli, G., Ngo, B., Warner, M. J., Olivere, L., Ridge, S. M., Jablonski, E. M., Therrien, J., Tannheimer, S., *et al.* (2018). Leukaemia hijacks a neural mechanism to invade the central nervous system. *Nature* **560**, 55–60.

Yu, G. I., Jun, S. E., and Shin, D. H. (2017). Associations of VCAM-1 gene polymorphisms with obesity and inflammation markers. *Inflamm. Res.* **66**, 217–225.

Zhang, H., Patel, A., Wang, Y.-J., Zhang, Y.-K., Kathawala, R. J., Qiu, L.-H., Patel, B. A., Huang, L.-H., Shukla, S., Yang, D.-H., *et al.* (2017). The BTK inhibitor ibrutinib (PCI-32765) overcomes paclitaxel resistance in ABCB1- and ABCC10-overexpressing cells and tumors. *Mol. Cancer Ther.* **16**, 1021–1030.

Zhang, Z., Wang, W., and Valdar, W. (2014). Bayesian modeling of haplotype effects in multiparent populations. *Genetics* **198**, 139–156.